Scanning tunnelling microscopy studies of Tsai-type quasicrystal approximants

Sam Coates,[1] Amnah Alofi,[1,2] Dominic Burnie,[1] Ronan McGrath,[1] and Hem Raj Sharma[1]

[1] *Surface Science Research Centre and Department of Physics, University of Liverpool, Liverpool L69 3BX, UK**

[2] *Albaha University, Al RAIB Al Bahah, 65528 2420 65528, Saudi Arabia*

(Dated: September 21, 2023)

We review scanning tunnelling microscopy (STM) studies of the surfaces of periodic Tsai-type approximants. Although they are useful analogues to the Tsai-type quasicrystals, the surfaces of these periodic approximants behave in subtly different and often more complex ways when compared to their quasiperiodic cousins. We present a summary of STM studies conducted upon Tsai-type approximants; we discuss the various differences and similarities between phases and surface directions, and compare these to the surfaces of the related quasicrystalline phases. We also present open questions which have been raised by these studies, and offer potential routes to answer them.

I. INTRODUCTION

Periodic approximants have been a vital tool for understanding quasiperiodic intermetallic alloys. Their periodicity allows for efficient theoretical exploration, with findings which have been applied to quasiperiodic systems without any loss of validity (e.g. [1–5]). Similarly, as they often share identical building blocks, deep understanding of the structural intricacies of approximants can lead to better comprehension of the quasiperiodic phases [6–8]. Periodic approximants have been determined for every quasicrystal (QC) alloy system, whether icosahedral (e.g. [7, 9–14]) or decagonal (e.g. [15–20]), and are routinely found in soft matter/2D systems [21–24]. From a high-level perspective, approximants can be consistently relied on as a simple (yet complex themselves) analogue to QCs across a wide range of systems and phases of matter.

However, when it comes to exploring the surfaces of approximants with scanning tunnelling microscopy (STM), we are dealing with a very local chemical and electronic environment, and changes to the underlying structure of the material/phase can have a significant impact on these environments. A wide array of periodic approximant surfaces and interfaces have been explored by STM; there comprehensive studies exploring approximants to icosahedral [25–29] and decagonal [30–35] QC phases, with an extensive series on 2D dodecagonal oxide QCs [22–24, 36–39]. While these studies have demonstrated that there are similarities between periodic approximant and QC surfaces (or interfaces), there are also enough differences that we can and should often treat these as separate classes of materials/surfaces.

In this review, we will focus on the results obtained from one family of approximants - the icosahedral Tsai-types. Tsai-type approximants are a broad class of intermetallic alloys that share the same building block: Tsai-type clusters [40]. These hierarchical clusters consist of a nesting structure of successively larger atomic shells, starting with a tetrahedron (or single atom depending on the phase [41]), which is contained successively within a dodecahedron, an icosahedron, an icosidodecahedron, and a rhombic triacontahedron, respectively. A schematic diagram is shown in Figure 1, where arrows indicate how the shells are nested, with the 2$^{\text{nd}}$ shell in yellow, 3$^{\text{rd}}$ in green, 4$^{\text{th}}$ in blue, and 5$^{\text{th}}$ in red. The tetrahedron is not shown as these atoms are most commonly not observed during surface studies; their dynamic motion leads to an ill–defined surface contribution [42–44].

The Tsai-type clusters can then decorate either a periodic or icosahedral quasiperiodic three-dimensional tiling, depending on whether we are exploring an approximant or quasicrystalline phase. There are a range of approximant types, which can be classified in order of their structural complexity, or, how close they approximate the QC phase. This classification depends on the ratio of two integers, q and p, which describe the orientation of the projection matrix used to obtain structural models from 6D [45]. q and p are successive numbers in the Fibonacci sequence, so that as q/p approaches τ, the golden ratio ($\frac{1+\sqrt{5}}{2}$), we get closer to the icosahedral QC phase. The periodic phases can therefore be referred to as 1/1, 2/1, 3/2 etc. Figures 1(b, c) show arbitrarily-sized, cubic unit cells of a 1/1 Tsai-type approximant, viewed along the [100] and [111] directions, respectively. The 1/1 phase can be considered as interpenetrating Tsai-type clusters which decorate the body-centre and vertices of such a cubic unit cell.

The binary quasicrystalline Cd-Yb alloy was the first Tsai-type discovered [46] – and there has since been a proliferation of ternary (and higher) periodic approximant and QC phases obtained by swapping out either Cd and Yb (or both) for other constituents, such that we have seen a rapid discovery of a range of phases. In tandem with these discoveries has been a concerted effort to refine our structural models of these systems, with chemical and structural disorder a common theme for exploration (e.g. [47–54]). Such a deep understanding of the structure of Tsai–type materials has allowed for in–depth interpretations of phase–specific and

* Corresponding author: samuel.coates@liverpool.ac.uk

stoichiometric–specific exotic behaviours, including magnetic transitions [55–58], novel electronic properties [59–61], and superconductivity [52, 62, 63].

The broad range of properties which are observed (or not) are therefore affected by the subtle structural, chemical, and electronic changes in different phases of the same family of materials. It is not unreasonable to suggest that we should expect to see an equally broad range of phase-dependent properties at the surfaces of these phases. However, the range of explored phases is very limited compared to the broad range of Tsai-type approximant phases which exist. While we are restricted by requiring low-vapour pressures for all constituents (i.e. to be compatible for ultra-high vacuum [UHV] study), we have yet to explore anything higher-order in complexity than 1/1 Tsai-type approximants (aside from the QC phase). In fact, despite their relative structural simplicity, there has been less work dedicated to exploring Tsai-type approximant surfaces when compared to the QC phase surfaces. It appears that we actually seem to have a better understanding of the aperiodic analogue compared to the periodic, as the lessons we have learnt from QC surfaces are often applied in our exploration of approximants [26–29, 31]. Similarly, there are still some unanswered questions on the behaviour of approximant surfaces.

In this review we will summarise results obtained from periodic Tsai-type approximant surfaces using STM, discuss the challenges and open questions that are faced with these systems, and present results from a new surface facet and phase. In section II we will discuss the basic recipe required to produce a surface for STM investigations. In section III we will summarize experimental STM results on Tsai-type approximants, before finally discussing open questions and concluding our review.

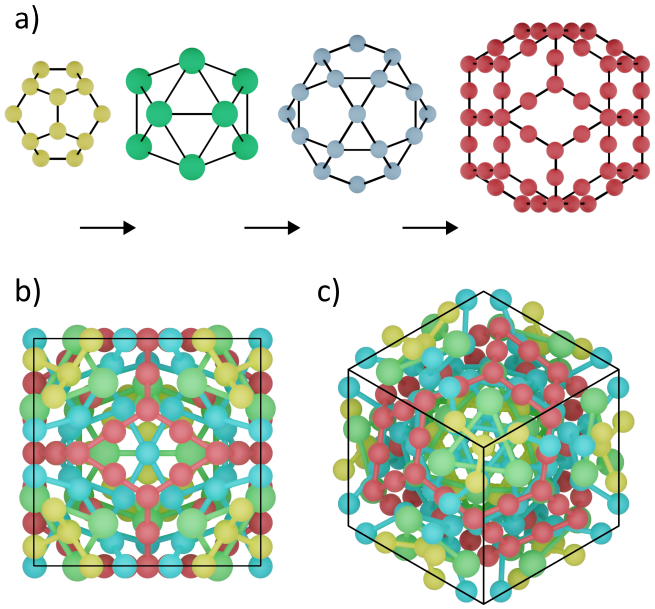

FIG. 1: **(a)** The Tsai type cluster, a hierarchical system of nested atomic shells. The 1st shell, not shown, is either a tetrahedron or a single atom. The 2nd shell, in yellow, is a dodecahedron, the 3rd, in green, an icosahedron, the 4th, in blue, an icosidodecahedron, and the 5th, in red, a rhombic triacontahedron. The spheres represent their atomic decoration. **(b)** The 1/1 Tsai-type approximant unit cell, as viewed perpendicular to the [100] direction. **(c)** The unit cell viewed perpendicular to the [111] direction.

II. EXPERIMENTAL DETAILS

Each of the crystals we discuss were grown as single-grain samples using the self-flux method, with specifics on size and quality discussed in each section. Here, we describe the general methods that we use to clean the samples for investigation under STM.

Once the desired surface facet is obtained (either through machine-cut or coarse-grain abrasion) samples are hand-polished with diamond paste of successively finer grades, typically going from: 6 μm, to 1 μm, and 0.25 μm. After ∼20 minutes of polishing in a figure-8 pattern at each grade, samples are placed in a beaker with solvent (typically methanol) and placed in an ultrasonic bath for ∼5 minutes, before repeating this process at the next finest grade. The figure-8 pattern is chosen to reduce preferential polishing along a specific direction, which may induce surface mis-cuts. Upon insertion into an ultra-high vacuum chamber, the surface of the sample is then further cleaned with sputter-anneal cycles. For all types of approximants (and indeed QCs), 30 min Ar^+ sputters are sufficient, with a typical drain current of ∼5-8μA, before annealing for ∼2–3 hours. For Tsai-type approximants, this is typically ∼450 °C. Surface temperatures are measured using a pyrometer with emissivity set to 0.35. Substrate cleanliness and ordering is then monitored with low-energy electron diffraction (LEED) or STM.

III. STM STUDIES OF TSAI-TYPE APPROXIMANTS

In this section we discuss results for the 1/1 Ag-In-Yb approximant, and then the 1/1 Au-Al-Gd/Tb systems. Before discussing these specific systems, we can first summarize the various properties which appear to be loosely consistent across the different Tsai-type approximant phases and surface terminations that have been explored. Table I summarizes the Tsai-type approximant and QC surfaces that have been explored, alongside specific remarks on these investigations. Results from the 1/1 Au-Al-Gd (110) surface will be published elsewhere, but a summary of initial findings are also shown in Table I.

Summary of STM studies on Tsai-type approximants

Phase	Surface	References	Experimental remarks
1/1 Ag-In-Yb	(100)	Cui et. al [25] Nozawa et. al [64]	Large terraces (> 100 nm) Poor resolution of finer atomic features Impurity phase observed
1/1 Ag-In-Gd	(100)	Hars et. al[26] Hars et. al [27]	Small terraces (< 100 nm) Heavily facetted Resolution dependent on facets
1/1 Ag-In-Tb	(100)	Hars et. al [27]	Same as Ag-In-Gd
1/1 Ag-In-Ca	(001)	Nozawa et. al [65]	n/a
1/1 Au-Al-Tb	(111)	Coates et. al [28]	Bias dependency (Tb at positive bias, Au/Al at negative) Reconstructed Au/Al atoms form a linear structure
1/1 Au-Al-Gd	(110)	Alofi, A. [66]	Small terraces (< 100 nm) formed by puckered planes containing Gd Heavily facetted Bias dependency (Gd at positive bias, Au/Al at negative)
QC Ag-In-Yb	2-fold	Cui et. al[67] Burnie et. al [68]	Large terraces (> 100 nm) Sub-cluster resolution of finer atomic features Bias dependency (Yb at positive bias, Ag/In at negative)
QC Ag-In-Yb	3-fold	Cui et. al [69]	Large, often incomplete terraces (> 100 nm), Sub-cluster resolution of finer atomic features Bias dependency (higher resolution at positive bias)
QC Ag-In-Yb	5-fold	Sharma et. al [70]	Large terraces (> 100 nm) Sub-cluster resolution of finer atomic features Bias dependency (Yb at positive bias, Ag/In at negative)

TABLE I: A summary of the work exploring the surfaces of different approximant and QC phases in the Tsai-type family.

A. 1/1 Ag-In-Yb (100)

The 1/1 Ag-In-Yb approximant can be grown as a mm-sized single grain, allowing the surface to be machine-cut and polished along a desired crystallographic direction. However, currently, only the (100) surface of this system has been investigated.

The 1/1 Ag-In-Yb(100) surface can be prepared with large terraces, comparable to those of simple periodic metals or quasicrystals. However, the surface termination depends on the method of surface preparation. There are two distinct types of atomic planes perpendicular to [100]: puckered layers with low atomic density and flat layers with high atomic density. Annealing the surface at lower temperatures results in terraces on both layers. However, at higher annealing temperatures, the puckered layers disappear, indicating their lower stability [71].

Despite the presence of large and flat terraces, achieving atomic resolution using STM on this surface is not attainable. The smallest features observed in STM have a diameter of approximately 1 nm for all tunnelling parameters, representing a group of atoms rather than individual atomic resolution, which we discuss further below.

B. 1/1 Ag-In-Gd/Tb (100)

The 1/1 Ag-In-Gd and 1/1 Ag-In-Tb approximant samples cannot be grown to the same size as the 1/1 Ag-In-Yb sample, despite using the same growth method, the self-flux method, for all the samples. Due to their small size, it is not practical to machine-cut these samples along desired planes. However, the flux method does yield samples with naturally developed facets along high symmetry directions. Therefore, these samples were hand-polished along the naturally occurring surfaces before undergoing surface preparation under UHV conditions.

Unlike machine-cut surfaces, hand polishing may introduce surface mis-cuts that induce surface faceting.

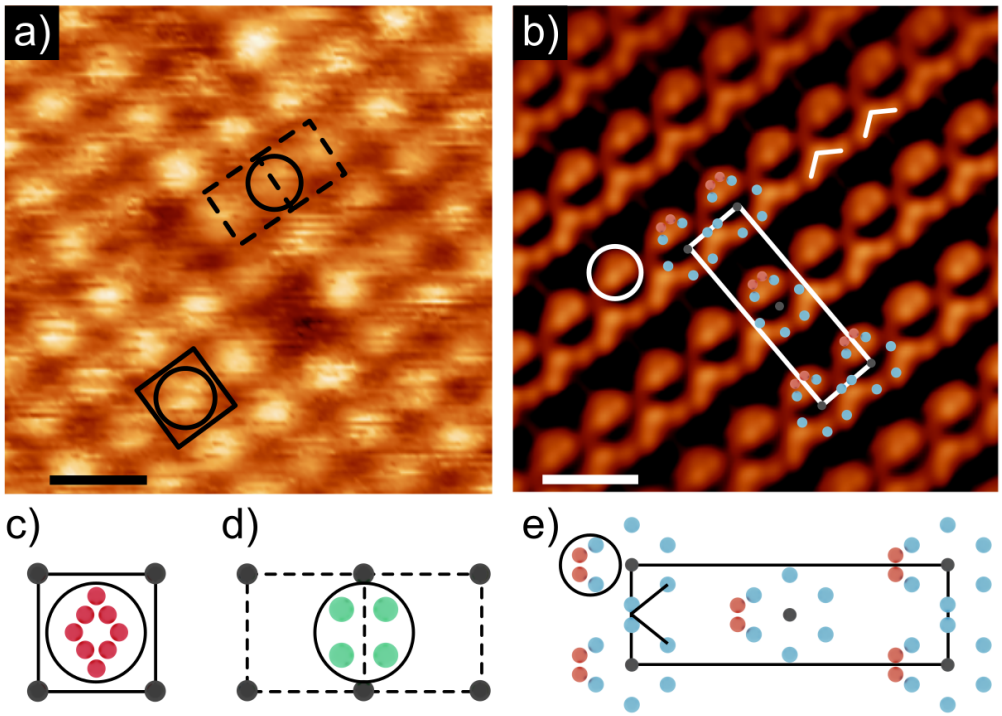

FIG. 2: **(a)** An STM image (V_b = 1 V, I_t = 0.18 nA) of the 1/1 Ag-In-Tb (100) surface showing cluster resolution. Two protrusions are marked, which are competing models for explaining the bright protrusions observed at the surface. The circle inside the square refers to a collection of 5^{th} shell atoms arranged in a diamond. The dashed rectangle refers to a square of 3^{rd} shell atoms. Scale bar is 2 nm. **(b)** An STM image (V_b = -2 V, I_t = 0.21 nA) of the (310) facet of 1/1 Ag-In-Tb showing sub-cluster resolution. A unit cell, bright protrusions, and chevron features are marked in white. The bright and chevron features are formed by 4^{th} and 5^{th} shell atoms. **(c)** The 5^{th} shell atom model used to explain the protrusions in **(a)**. **(d)** The competing 3^{rd} shell atom model used to explain the protrusions in **(a)**. **(e)** The 4^{th} and 5^{th} shell model used to explain the features observed in **(b)**. A circle and chevron match with the corresponding features in **(b)**. Scale bar is 2 nm.

Such surface mis-cut-induced faceting has been observed on the (100) surface of both of these approximants [26]. STM and LEED studies revealed the presence of facets along various crystallographic directions such as (100), (310), (3$\bar{1}$0), (301), (30$\bar{1}$), (411), (4$\bar{1}\bar{1}$), (501), and (710). The development of these facets appears to be driven by the atomic density, chemistry, and bonding between atoms in these planes. The facet planes are enriched with In atoms, which are bonded with Gd/Tb atoms. While these planes exhibit a relatively high atomic density, it is still lower than that of the close-packed (111) planes. Consequently, the nearest-neighbour distance between atoms in the topmost layer is typically larger than their atomic diameters. Therefore, these atoms must be bonded with subsurface atoms, which highlights the role of subsurface atoms in surface stability in these facets.

The different chemical/electronic environments produced through these facets also appear to have an effect on the resolution we can obtain via STM. Rather than recap each facet, we can quickly compare the structures observed from the (100) and (310) facets of the 1/1 Ag-In-Tb approximant.

Figure 2(a) shows an STM image of the 1/1 Ag-In-Tb (100) surface, which only shows features with a diameter of 1 nm arranged in a square lattice, similar to those observed on the 1/1 Ag-In-Yb(100) surface. Again, these are the only features observed for all tunnelling parameters. Knowing that the step–terrace morphology of this surface forms at planes which intersect the cluster-centre of the Tsai-type clusters, there are two models which can explain these features. The first case is that a diamond arising from the 5^{th} shell contributes to the tunneling current producing the protrusions, shown with reference to the unit cell in Figure 2(c). The second is that the atoms of two neighbouring unit cells form a square of 3^{rd} shell atoms such as in Figure 2(d). Both of these examples are overlaid on Figure 2(a) with reference to the position of the protrusion in terms of the unit cell.

In contrast, we observe sub-cluster resolution on the 1/1 Ag-In-Tb (310) facet, as shown in the STM image in Figure 2(b). Here, a row-like structure is observed, where bright rows can be decomposed into two smaller rows which consist of two different types of protrusions. These are highlighted in Figure 2(b) as a white circle and

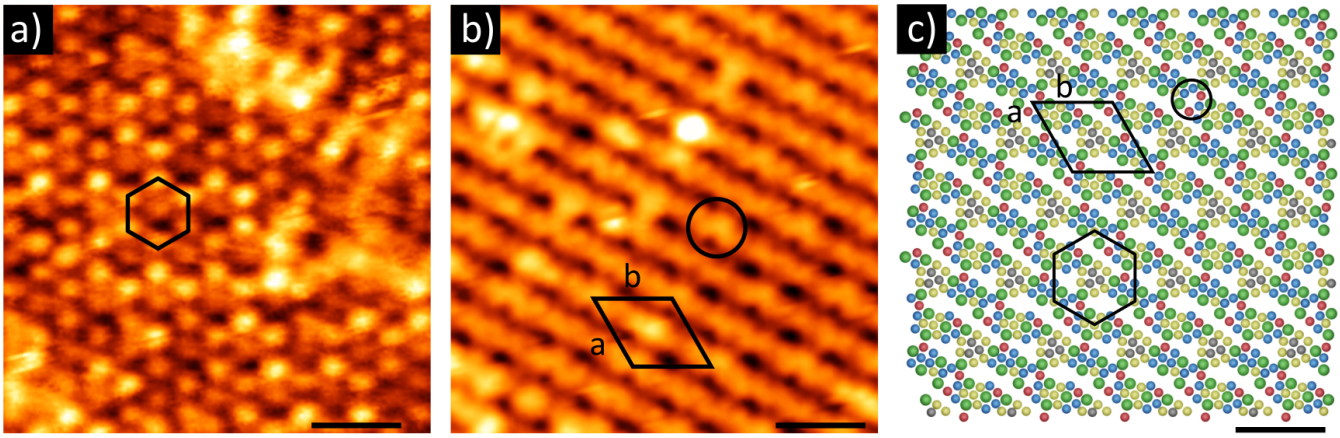

FIG. 3: **(a)** An STM image (V_b = 1 V, I_t = 0.175 nA) of the 1/1 Au-Al-Tb (111) surface at positive bias, showing the Tb-resolved surface. Bright dimer–like protrusions form a hexagonal structure. Scale bar is 3 nm. **(b)** STM image (V_b = -1 V, I_t = 0.140 nA) of the surface under negative bias. A rhombohedral unit cell is marked, linking v–shaped protrusions, one of which is circled in black. Scale bar is 3 nm. **(c)** Model schematic of **(a)**. Red, blue, yellow, and grey circles indicate 5$^{\text{th}}$, 4$^{\text{th}}$, 2$^{\text{nd}}$, and 1$^{\text{st}}$ shell positions of Au/Al atoms. The hexagon from **(a)**, rhombohedral unit cell and v–shaped protrusions of (**b**) are marked. Scale bar is 3 nm.

white chevrons. These features are ascribed to a collection of 4$^{\text{th}}$ and 5$^{\text{th}}$ shell atoms, with the unit cell overlaid on Figure 2(b) and shown in detail in Figure 2(e). Here, two 5$^{\text{th}}$ shell atoms and two atoms from a 4$^{\text{th}}$ shell hexagon form the circle feature, while the remaining 4$^{\text{th}}$ shell atoms in the hexagon form the chevron structure. Similar sub-cluster resolution was also observed on the $(3\bar{1}0)$, (301), $(30\bar{1})$, and (501) facets, but not the (411), $(4\bar{1}\bar{1})$, (710) planes. These results suggest that the likelihood of obtaining sub-cluster resolution in these systems depends very strongly on the local chemical environment of specific atoms.

C. Au-Al-Tb (111)

The investigation of the 1/1 Au-Al-Tb (111) surface represented the first surface exploration on a non-Ag/In containing Tsai-type phase, and was instigated after the exhibition of an antiferromagnetic phase transition [56] – with a long-term view to explore its magnetic surface structure via spin-polarized STM. Similarly, it was the first Tsai-type (111) surface to be explored, and was chosen as it is an analogue to the 3-fold surface of an icosahedral Tsai-type QC.

Under STM, the morphology of the surface showed a Tb–terminated step–terrace structure, with step heights appearing to minimize the number of 'broken' bulk icosahedra. Here, we mean that terraces were formed by slabs of atoms that were separated by step heights of ∼1.22 nm, despite there being geometrically and chemically equivalent surface planes in-between the slabs separated by this large step. To be specific, the separation between equivalent atomic planes or slabs, d = 0.85 nm, where:

$$d_{(hkl)} = \frac{a}{\sqrt{h^2 + k^2 + l^2}} \tag{1}$$

is the separation between planes in the bulk, and a is the lattice constant. The observation of step heights $1.5 \times d$ suggested, then, that there was another driving force for these step heights beyond the terrace constituents and their arrangement. In brief, we calculated the number of whole icosahedra in a section of the bulk for small and large step heights, for 5 step heights each. Atoms were then removed to simulate a step–terrace structure with 5 steps, and the number of whole icosahedra was counted - where the larger step height value gave 2.5 times as many unbroken icosahedra in the bulk. Therefore, we suggested that minimizing broken icosahedra was important for surface stability.

Investigation of the finer structure of terraces showed the first surface reconstruction in a Tsai-type approximant. In general, the observed atomic structure of the terraces was bias dependent, with Tb atoms imaged under positive bias and Au/Al atoms under negative bias. Figures 3(a,b) show STM images of the surface under positive and negative bias, respectively. At positive bias, we resolved a hexagonal structure which was found to arise from triangles of Tb atoms, formed either by the tops or bottoms of the (111)-aligned icosahedra - these features are highlighted in Figures 3(a,c) by black hexagons, where the model structure links triangles of Tb atoms coloured in green. Under negative bias we observed a linear row structure, such that we consider the surface to be reconstructed. Here, v-shaped protrusions which consist of 4$^{\text{th}}$ and 5$^{\text{th}}$ shell atoms formed a rhombohedral unit cell which can be related back to the hexagonal nature of the surface plane. An example of

one such protrusion is highlighted by a circle in Figure 3(b,c) (blue circles are 4^{th} shell atoms, red circles are 5^{th}), as well as the rhombohedral unit cell it forms. The reconstruction was explained by the removal of certain 4^{th} and 5^{th} shell atoms which was supported by density functional theory (DFT) calculations [28], which reproduced a stable reconstructed surface and simulated STM images at positive and negative bias.

IV. DISCUSSION AND SUMMARY

We have presented the current state of STM studies of Tsai-type approximants, which we hope can act as a consolidated guidebook for further explorations into these systems, in particular, the summary of studies in Table I. In summary, across a range of surface symmetries and chemistries we find three common features in STM studies of Tsai-type approximants: first, each high-symmetry surface which has been explored terminates at dense planes which contain RE atoms, including the QC phase. This phenomenon has been attributed to the low surface free energy and low-lying unoccupied 3d states of rare-earth (RE) atoms, which contribute to surface stabilisation [65, 67, 72]. Similarly, STM bias-dependency is observed more often than not, where RE atoms typically dominate the density of states when probing with positive bias (and vice versa).

Second, and with one exception (the 1/1 Au-Al-Gd (110) surface [66]), all surface planes intersect directly with the centre of the Tsai-type cluster, which is also true for the QC phase. However, this is a slightly obvious point, as there are only a limited number of planes where RE-dense planes and cluster-centres lie perpendicular to the surface direction under investigation.

Third, in general, the quality of these approximant surfaces is poor in comparison to the QC phase, that is, terraces are smaller, there are more incomplete terraces, and defect sites within the terraces are more prevalent. Exactly why this is the case is unclear at this point. While it may be tempting to describe the approximant surfaces as less stable than those of the QC phase (and perhaps as a direct consequence of their structure), it is important to note that each of the approximant phases we have discussed in this review have been grown using the self-flux method, whereas the QC phase which has been used for surface studies was grown using the Bridgman method [70, 73]. Previous work has showed little difference between the surfaces of approximants grown using these two methods [29], but it is a key parameter which differentiates the samples under question. However, the clear route to at least establishing whether there is a trend with structural complexity and surface quality is to explore higher-order approximants. Likewise, changing the constituents of the phase is another parameter which may be key.

As we have demonstrated, there is still a rich environment to explore, as changes in chemistry and surface orientation can often bring about different surface behaviour in these systems. The specific driving force behind these changes, and how (or if) these changes can be related to the quasicrystalline Tsai-type phase are still open questions. As we can easily control these parameters, it is likely these questions can, in fact, be answered. Looking forward, is natural to suggest that a systematic approach to investigating different phase, orientation, and approximant complexity (2/1 etc.) is the route to a full understanding of the surfaces of these materials.

V. ACKNOWLEDGEMENTS

S.C and H.R.S wrote the manuscript, S.C prepared the figures. H.R.S and R.M conceptualized the review. This work was supported by EPSRC grant EP/X011984/1 (S.C).

[1] E. Cockayne, R. Phillips, X. B. Kan, S. C. Moss, J. L. Robertson, T. Ishimasa, and M. Mori. *Journal of non-crystalline solids*, 153:140–144, 1993.
[2] M. Krajčí, M. Windisch, J. Hafner, G. Kresse, and M. Mihalkovič. *Phys. Rev. B*, 51(24):17355, 1995.
[3] M. Windisch, M. Krajčí, and J. Hafner. *Journal of Physics: Condensed Matter*, 6(35):6977, 1994.
[4] M. Krajčí, J. Hafner, and M. Mihalkovič. *Physical Review B*, 55(2):843, 1997.
[5] M Krajčí, J Hafner, and M Mihalkovič. *Physical Review B*, 62(1):243, 2000.
[6] P. Guyot and M. Audier. *Philosophical Magazine B*, 52(1):L15–L19, 1985.
[7] V. Elser and C. L. Henley. *Phys. Rev. Lett.*, 55(26):2883, 1985.
[8] Z. He, H. Li, H. Ma, and G. Li. *Scientific reports*, 7(1):40510, 2017.
[9] T. Ishimasa, Y. Tanaka, and S. Kashimoto. *Philosophical Magazine*, 91(33):4218–4229, 2011.
[10] T. Takeuchi and U. Mizutani. *Physical Review B*, 52(13):9300, 1995.
[11] X. Zhang, R. M. Stroud, J. L. Libbert, and K. F. Kelton. *Philosophical Magazine B*, 70(4):927–950, 1994.
[12] A. Quivy, M. Quiquandon, Y. Calvayrac, F. Faudot, D. Gratias, C. Berger, R. A. Brand, V. Simonet, and F. Hippert. *Journal of Physics: Condensed Matter*, 8(23):4223, 1996.
[13] A. Palenzona. *Journal of the Less Common Metals*, 25(4):367–372, 1971.
[14] C. P. Gómez and S. Lidin. *Angewandte Chemie International Edition*, 40(21):4037–4039, 2001.
[15] W. Steurer, T. Haibach, B. Zhang, S. Kek, and R. Lück. *Acta Crystallographica Section B*, 49(4):661–675, 1993.

[16] L. E. Levine, P. C. Gibbons, and A. M. Viano. *Philosophical Magazine B*, 70(1):11–32, 1994.

[17] V. Demange, J. S. Wu, V. Brien, F. Machizaud, and J. M. Dubois. *Materials Science and Engineering: A*, 294:79–81, 2000.

[18] T. L. Daulton and K. F. Kelton. *Philosophical magazine letters*, 63(5):257–265, 1991.

[19] X. Z. Li and K. H. Kuo. *Philosophical Magazine B*, 65(3):525–533, 1992.

[20] C. Dong, J. M. Dubois, S. S. Kang, and M. Audier. *Philosophical Magazine B*, 65(1):107–126, 1992.

[21] T. Dotera. *Israel Journal of Chemistry*, 51(11-12):1197–1205, 2011.

[22] S. Förster, S. Schenk, E. M. Zollner, O. Krahn, C. Cheng-Tien, F. O. Schumann, A. Bayat, K-M. Schindler, M. Trautmann, R. Hammer, et al. *Physica Status Solidi (b)*, 257(7):1900624, 2020.

[23] M. Maniraj, L. V. Tran, O. Krahn, S. Schenk, W. Widdra, and S. Förster. *Physical Review Materials*, 5(8):084006, 2021.

[24] S. Schenk, S. Förster, K. Meinel, R. Hammer, B. Leibundgut, M. Paleschke, J. Pantzer, C. Dresler, F. O. Schumann, and W. Widdra. *Journal of Physics: Condensed Matter*, 29(13):134002, 2017.

[25] C. Cui, H. Sharma, P. Nugent, M. Shimoda, and A. P. Tsai. *Acta Physica Polonica A*, 126(2):577–580, 2014.

[26] S. Hars, H. R. Sharma, J. A. Smerdon, T. P. Yadav, R. Tamura, M. Shimoda, and R. McGrath. *Acta Physica Polonica A*, 126(2):479–481, 2014.

[27] S. S. Hars, H. R. Sharma, J. A. Smerdon, T. P. Yadav, A. Al-Mahboob, J. Ledieu, V. Fournée, R. Tamura, and R. McGrath. *Phys. Rev. B*, 93(20):205428, 2016.

[28] S. Coates, K. Nozawa, M. Fukami, K. Inagaki, M. Shimoda, R. McGrath, H. R. Sharma, and R. Tamura. *Phys. Rev. B*, 102(23):235419, 2020.

[29] Fournée, V. and Ross, A. R. and Lograsso, T. A. and Anderegg, J. W and Dong, C. and Kramer, M. and Fisher, I. R. and Canfield, P. C. and Thiel, P. A. *Phys. Rev. B*, 66(16):165423, 2002.

[30] J. K. Parle, A. Beni, V. R. Dhanak, J. A. Smerdon, P. Schmutz, M. Wardé, M-G Barthés-Labrousse, B. Bauer, P. Gille, H. R. Sharma, et al. *Applied surface science*, 283:276–282, 2013.

[31] H. R. Sharma, M. Shimoda, V. Fournée, A. R. Ross, T. A. Lograsso, and A. P. Tsai. *Phys. Rev. B*, 71(22):224201, 2005.

[32] V. Fournée, É. Gaudry, M-C De Weerd, R. D. Diehl, and J. Ledieu. *MRS Online Proceedings Library (OPL)*, 1517:mrsf12–1517, 2013.

[33] S. G. Song and E. R. Ryba. *Philosophical Magazine B*, 69(4):707–724, 1994.

[34] W. Sun, T. Ohsuna, and K. Hiraga. *Journal of Alloys and Compounds*, 342(1-2):87–91, 2002.

[35] R. Addou, É Gaudry, Th. Deniozou, M. Heggen, M. Feuerbacher, P. Gille, Y. Grin, R. Widmer, O. Gröning, V. Fournée, et al. *Physical Review B*, 80(1):014203, 2009.

[36] F. E. Wührl, O. Krahn, S. Schenk, W. Widdra, and S. Förster. *Physical Review B*, 107(19):195414, 2023.

[37] C. R. Merchan, T. T. Dorini, F. Brix, L. Pasquier, M. Jullien, D. Pierre, S. Andrieu, K. Dumesnil, S. S. Parapari, S. Šturm, et al. *Physical Chemistry Chemical Physics*, 24(12):7253–7263, 2022.

[38] S. Förster, M. Trautmann, S. Roy, W. A. Adeagbo, E. M. Zollner, R. Hammer, F. O. Schumann, K. Meinel, S. K. Nayak, K. Mohseni, et al. *Physical Review Letters*, 117(9):095501, 2016.

[39] J. Yuhara, K. Horiba, R. Sugiura, X. Li, and T. Yamada. *Physical Review Materials*, 4(10):103402, 2020.

[40] H. Takakura, C. P. Gómez, A. Yamamoto, M. de Boissieu, and A. P. Tsai. *Nat. Mater.*, 6(1):58, 2007.

[41] S. Suzuki, A. Ishikawa, T. Yamada, T. Sugimoto, A. Sakurai, and R. Tamura. *Materials Transactions*, 62(3):298–306, 2021.

[42] H. Euchner, T. Yamada, S. Rols, T. Ishimasa, Y. Kaneko, J. Ollivier, H. Schober, M. Mihalkovic, and M. de Boissieu. *Journal of Physics: Condensed Matter*, 25(11):115405, 2013.

[43] C. P. Gómez and S. Lidin. *Phys. Rev. B*, 68(2):024203, 2003.

[44] K. Nishimoto, T. Sato, and R. Tamura. *Journal of Physics: Condensed Matter*, 25(23):235403, 2013.

[45] I. Buganski and J. Wolny. *Journal of Alloys and Compounds*, 939:168823, 2023.

[46] A. P. Tsai, J. Q. Guo, E. Abe, H. Takakura, and T. J. Sato. *Nature*, 408(6812):537, 2000.

[47] G. Gebresenbut, R. Tamura, D. Eklöf, and C. P. Gómez. *Journal of Physics: Condensed Matter*, 25(13):135402, 2013.

[48] G. Gebresenbut, M. S. Andersson, P. Beran, P. Manuel, P. Nordblad, M. Sahlberg, and C. P. Gómez. *Journal of Physics: Condensed Matter*, 26(32):322202, 2014.

[49] G. H. Gebresenbut, M. S. Andersson, P. Nordblad, M. Sahlberg, and C. P. Gómez. *Inorganic Chemistry*, 55(5):2001–2008, 2016.

[50] G. Gebresenbut, T. Shiino, D. Eklöf, D. Ch. Joshi, F. Denoel, R. Mathieu, U. Häussermann, and C. P. Gómez. *Inorganic chemistry*, 59(13):9152–9162, 2020.

[51] S. Ghanta, U. Häussermann, and A. Rydh. *Journal of Solid State Chemistry*, 327:124246, 2023.

[52] K. Deguchi, M. Nakayama, S. Matsukawa, K. Imura, K. Tanaka, T. Ishimasa, and N. K. Sato. *Journal of the Physical Society of Japan*, 84(1):015002, 2015.

[53] K. Tanaka, Y. Tanaka, T. Ishimasa, M. Nakayama, S. Matsukawa, K. Deguchi, and N. Sato. *Acta Physica Polonica A*, 126(2):603–607, 2014.

[54] T. Yamada, H. Takakura, M. De Boissieu, and A-P Tsai. *Acta Crystallographica Section B: Structural Science, Crystal Engineering and Materials*, 73(6):1125–1141, 2017.

[55] R. Tamura, Y. Muro, T. Hiroto, K. Nishimoto, and T. Takabatake. *Phys. Rev. B*, 82(22):220201, 2010.

[56] A. Ishikawa, T. Fujii, T. Takeuchi, T. Yamada, Y. Matsushita, and R. Tamura. *Phys. Rev. B*, 98(22):220403, 2018.

[57] S Yoshida, S Suzuki, T Yamada, T Fujii, A Ishikawa, and R Tamura. *Phys. Rev. B*, 100(18):180409, 2019.

[58] R. Tamura, A. Ishikawa, S. Suzuki, T. Kotajima, Y. Tanaka, T. Seki, N. Shibata, T. Yamada, T. Fujii, C-W. Wang, et al. *Journal of the American Chemical Society*, 143(47):19938–19944, 2021.

[59] K. Deguchi, S. Matsukawa, N. K. Sato, T. Hattori, K. Ishida, H. Takakura, and T. Ishimasa. *Nat. Mat.*, 11(12):1013–1016, 2012.

[60] T. Watanuki, S. Kashimoto, D. Kawana, T. Yamazaki, A. Machida, Yukinori Tanaka, and Taku J. S. *Phys. Rev.*

B, 86(9):094201, 2012.

[61] S. Jazbec, S. Vrtnik, Z. Jagličić, S. Kashimoto, J. Ivkov, P. Popčević, A. Smontara, H. J. Kim, J. G. Kim, and J. Dolinšek. *Journal of Alloys and Compounds*, 586:343–348, 2014.

[62] K. Kamiya, T. Takeuchi, N. Kabeya, N. Wada, T. Ishimasa, A. Ochiai, K. Deguchi, K. Imura, and N. K. Sato. *Nat. Commun.*, 9(1):1–8, 2018.

[63] K. Deguchi, M. Nakayama, S. Matsukawa, K. Imura, K. Tanaka, T. Ishimasa, and N. K. Sato. *Journal of the Physical Society of Japan*, 84(2):023705, 2015.

[64] K. Nozawa. *To be published*, 2023.

[65] K. Nozawa and Y. Ishii. 226(1):012030, 2010.

[66] Amnah Alofi. *Surfaces of Complex Metallic Alloys and Their Adsorption Properties*. PhD thesis, University of Liverpool, 2023.

[67] C. Cui, P. J. Nugent, M. Shimoda, J. Ledieu, V. Fournée, A. P. Tsai, R. McGrath, and H. R. Sharma. *Journal of Physics: Condensed Matter*, 26(1):015001, 2013.

[68] D. Burnie, S. Coates, R. McGrath, and H. R. Sharma. *Journal of Physics: Conference Series*, 1458:012017, jan 2020.

[69] C. Cui, P. J. Nugent, M. Shimoda, J. Ledieu, V. Fournée, A. P. Tsai, R. McGrath, and H. R. Sharma. *Journal of Physics: Condensed Matter*, 24(44):445011, 2012.

[70] H. R. Sharma, M. Shimoda, S. Ohhashi, and A. P. Tsai. *Philos. Mag.*, 87(18-21):2989–2994, 2007.

[71] C. Cui, M. Shimoda, and A. P. Tsai. *RSC Advances*, 4(87):46907–46921, 2014.

[72] Y. Ishii and T. Fujiwara. *Phys. Rev. Lett.*, 87(20):206408, 2001.

[73] H. R. Sharma, M. Shimoda, K. Sagisaka, H. Takakura, J. A. Smerdon, P. J. Nugent, R. McGrath, D. Fujita, S. Ohhashi, and A. P. Tsai. *Phys. Rev. B*, 80(12):121401, 2009.